Editorial Manager(tm) for Rock Mechanics and Rock Engineering
Manuscript Draft

Manuscript Number: RMRE-D-10-00111R1

Title: Correlations developed for estimation of hydraulic parameters of rough fractures through the simulation of JRC flow channels

Article Type: Original Paper

Keywords: Fracture surface roughness; Riemannian roughness parameter; pressure drop; JRC flow channels; fracture closure; FLUENT

Corresponding Author: Vamegh Rasouli, PhD

Corresponding Author's Institution:

First Author: Vamegh Rasouli, PhD

Order of Authors: Vamegh Rasouli, PhD;Armin Hosseinian, PhD

Response to Reviewers: The corrections suggested by the Editor in chief of the journal have been applied. The references are now in name/year format within the text and also the m/s has been reviewed professionally for its english.

Correlations developed for estimation of hydraulic parameters of rough fractures through the simulation of JRC flow channels

V. Rasouli & A. Hosseinian

Curtin University of Technology, Australia

Abstract

The hydro-mechanical response of fractured rock masses is complex, due partly to the presence of fractures at different scales. Surface morphology has a significant influence on fluid flow behaviour of a fracture. Different empirical correlations and statistical models have been proposed to estimate the equivalent hydraulic aperture and determine the pressure drop along a fracture. However, the existing models suffer from not being adequately generalised to be applicable to a wide range of real fracture surfaces.

To incorporate the effect of profile roughness in the hydro-mechanical behaviour of fractured rock masses, the joint roughness coefficient (JRC) is the most widely used empirical approach. However, the average JRC of two fracture walls in fluid flow analysis, as is a common practice, appears to be inappropriate. It will be shown how different combinations of pairs of JRCs could lead to a similar JRC value. Also, changing the position of the top and bottom walls of a fracture can significantly change the hydraulic response of the fracture while the average JRC is identical in both cases.

In this paper, correlations are developed which are based on the simulation of JRCs using estimated fluid flow parameters of 2D fractures can be estimated. In order to widen the application range of the correlations, JRC flow channels were generated: these are 2D channels with their top and bottom walls being made from two of the JRC profiles. To estimate the JRC of linear profiles a correlation developed between JRC and a newly developed Riemannian roughness parameter, D_{R1}, is proposed. Considering ten JRC profiles, a total of 100 JRC flow channels were generated. In order to only investigate the effect of surface roughness on fluid flow, the minimum closure between the top and bottom walls of JRC flow channels were considered to be constant. Three cases with minimum closures of 0.01, 0.05 and 0.10cm were considered in this study. All JRC flow channels were subjected to fluid analysis using FLUENT software. Based on these results, correlations were developed between the geometrical and hydraulic properties of flow channels. Analysis of several real fractures demonstrated the applicability of these correlations.

Keywords

Fracture surface roughness, Riemannian roughness parameter, pressure drop, JRC flow channels, fracture closure, FLUENT

1 Introduction

The analysis of fluid flow through natural fractures is a common area of research in different disciplines with a wide range of applications from mining and civil to petroleum engineering. For example, production of fluids from a naturally fractured reservoir is closely related to transmissivity of the fracture network (Wayne and Schechter, 2006). Amongst the various parameters affecting flow of a fluid through a fracture, the effect of surface morphology, or roughness, appears to be very important (Zimmerman and Bodvarsson, 1996). Considering a single fracture with a constant mechanical aperture, one can recognise how an increase in roughness could lead to a lesser ability of fluid to pass through the fracture, or a higher pressure drop. Now assuming surfaces having with similar mean mechanical aperture but dissimilar geometries (e.g. synthetic profiles with sinusoidal or triangular asperities), different flow responses maybe expected if they are subjected to fluid flow. This simple example illustrates the complexity associated with fluid flow analysis with respect to surface roughness.

Several analytical models, numerical methods and laboratory experiments have been developed to study the effect of surface roughness on fluid flow through a single fracture (Komaya et al., 2009; Petchsingto, 2009; and Liu, 2005). Several attempts use the Cubic law concept, which is a model developed for smooth channels. The presence of surface roughness, however, causes a deviation from the Cubic law. In rough channels, or rock fractures such as in this study, aperture asperity heights are distributed irregularly and they are not constant along the profile geometry. This makes it difficult to assign a unique value for the aperture of the channel (h) in the Cubic law equation. This is significant as the aperture appears with cubic power in the Cubic law equation. Several attempts have been made to introduce an appropriate value for the equivalent opening (hydraulic aperture) of a rough channel to be used in the Cubic law (Zimmerman and Bodvarsson, 1991). Also, different correlations have been reported to link the hydraulic aperture h_H to the fracture mechanical aperture h_m (Yeo, 2005; Kolditz, 2001; Yeo, 2005; Ge, 1997 and Renshaw, 1995).

In addition to the mean aperture parameter, other empirical and statistical parameters have been proposed to consider the effect of surface roughness. In a very recent attempt,

Rasouli and Harrison (2010) proposed a 1D Riemannian roughness parameter, D_{R1}, as a quantitative approach for roughness assessment of linear profiles. This parameter has been developed using the analysis of the distribution of unit normal vectors to the profile.

The joint roughness coefficient (JRC) proposed by Barton and Choubey(1978) is perhaps the most commonly used parameter for quantifying fracture surface roughness. Several attempts have been made to correlate JRC with hydraulic behaviour of fractures before and after fracture shearing, for example the ratio of hydraulic to mechanical aperture (Barton, 2007; Olson and Barton, 2001; Barton and Quadros, 1997) and fracture hydraulic conductivity (Scesi and Gattinoni, 2007).

The necessity for performing 3D analysis of fluid flow in rock fractures in order to avoid very small or zero openings which leads to unrealistic fluid flow response in a 2D channel is important and has been discussed by different people (e.g. Komaya et al., 2009; Crandall et al., 2010a; Crandall et al., 2010b; Kulatilake, 2008; Giacomini, 2008; Nazirdoust et al., 2006; Petchsingto, 2009; and Sarkar, 2002). In real situation, the fluid moves around very small openings and continues its flow whereas in a 2D channel there would be no fluid flow if the opening becomes zero. While this concept is well understood, the purpose of this paper is solely to analyse the JRC profiles and correlate their geometry with flow properties. The 2D analysis was performed using with an assumption that the channels have a minimum opening to avoid zero fluid flow. This allows comparison of different JRC profiles with respect to each other when they are subjected to fluid flow studies.

In this paper, to emphasize the importance of 3D analysis of fluid flow in rock fractures, the results of simulations of a synthetically generated fracture surface is presented. In the 2D analysis, first, a correlation is developed between JRC and D_{R1} which allows an estimation of JRC value of real rock profiles to be made. Then JRC is attempted to be correlated with the flow response of real rock profiles. For this, JRC flow channels are developed with a constant minimum closure distance between the two walls and these channels are subjected to flow analysis using FLUENT software. One of the 10 JRC profiles forms the top wall of a JRC flow channel with another JRC profile being the bottom wall. Three minimum closure distances of 0.01, 0.05 and 0.10 cm are chosen for this study and therefore a total of 300 flow channels will be analysed to investigate the flow response of a wide range of channels which are thought to be representative of real rock fractures. The results and correlations developed between the JRC and various fluid flow parameters are presented here.

2 3D versus 2D fluid flow analysis

As discussed in the previous section, fluid flow simulations of rock fractures must be performed in 3D in order to realistically examine the effect of fracture asperities on fluid flow behaviour. In 2D, the fluid is significantly influenced by the existence of very small openings along the fracture path: this will result in an unrealistic flow response compared to the 3D result where the fluid may freely move around small openings and continues its movement. While this has been studied and reported by many people in the past, here to emphasize this effect, we show the results of 3D fluid flow simulations for a synthetically generated surface. Figure 1 shows the fracture geometry which was generated using a random surface generation algorithm based on Gaussian statistics. The surface has an equal length and width of 15 cm in both *X* and *Y* directions, respectively. The asperity height distribution ranges between 0 and 0.2 cm, with a correlation distance of 1.0 cm used for surface generation. The data was generated with a preferred deviation along the *Y* axis, i.e. 90° direction in order to be able to compare the flow response in two orientations along *X* and *Y* directions.

Fluid flow simulations were carried out using FLUENT (see Section 6) for this synthetic channel. Figure 2 shows the velocity magnitudes for this channel for a fluid flowing in the *X* and *Y* directions at zero shear offset. The results shown in this figure belong to a *Z* plane and therefore, the white areas are the locations where this plane does not have any intersection with the fracture walls. From these figures, while it is seen that the flow behaviour is clearly direction dependent, the velocity magnitude changes significantly at different points depending on the distance between the two walls at different locations. The velocity magnitude reduces close to zero at locations where the opening distance is zero but the fluid continues to flow around this closed throat, as is seen at different locations in Figures 2.

If one performs a 2D analysis by considering a channel where the opening is zero at one or some points along the fluid path, it can be realised that the velocity magnitude becomes zero corresponding to this channel. This is not true in the real situation as explained above.

The sole purpose of the study in this paper is to investigate how the effect of fracture surface morphology on fluid flow can be represented by JRCs. Therefore, the simulations here are performed considering a minimum aperture for a 2D channel and focus the analysis on the effect of changing surface morphology, i.e. channels with different JRC.

3 JRC and flow response of fractures

Based on their extensive lab experiments, Barton and Choubey (1977) proposed 10 typical rock profiles with different roughness and waviness as being representative of real rock fracture geometries (Rasouli and Harrison, 2010). These profiles, ordered from the smoothest to the roughest, are assigned a JRC value changing between 1 and 20. By visual comparison of a real fracture surface, one should choose a profile with the closest geometry to the fracture and assign the same JRC value to the real fracture, as a measure of its roughness. The exemplar JRC profiles are shown in Figure 3. JRC has been correlated to mechanical and hydraulic properties of rock fractures. For this reason and also the simple application of this approach, JRC has been widely used in different rock engineering applications to study the hydro-mechanical properties of fractures. This is true while it is well known that the JRC is a subjective method and suffers from a number of deficiencies (Rasouli and Harrison, 2001; Liu and Sterling, 1990).

Barton et al. (1985) performed experimental analysis on the fluid flow coupled with shear-flow behaviour of rock fractures and compared their results with data used by other researchers. From this study they proposed following a correlation between mechanical aperture (h_m), and hydraulic aperture or theoretical parallel plate analogy (h_H) in relation to the JRC:

$$h_H = \frac{JRC^{2.5}}{\left(h_m / h_H\right)^2} \tag{1}$$

or

$$h_H = \frac{{h_m}^2}{JRC^{2.5}}. \tag{2}$$

In this equation, h_m and h_H are expressed in μm. One should note that this equation is only valid for $h_m \geq h_H$. From this equation and its graphical representation given in Figure 4, it is seen that as the fracture surface becomes rougher the difference between the mechanical and hydraulic aperture increases (i.e. larger h_m/h_H ratios). Also, the ratio of h_m/h_H even for smooth natural joints is likely to be higher than 1.0, which is believed to be due to the influence of the roughness and the tortuosity of the flow channel which causes an increase in the head losses. Figure 4 also shows that, even for very rough profiles, the influence of roughness and tortuosity decreases as the fracture opens and the ratio of h_m/h_H approaches 1.0.

In real applications one should estimate the JRC of the top and bottom walls of a fracture and then use equation 1 to obtain an estimation for the mean hydraulic aperture (h_H) of the fracture. The mean hydraulic aperture is then replaced with opening h in the Cubic law

equation which is for smooth channels to estimate the pressure drop along a fracture. The Cubic law is represented as (Jaeger et al., 2007):

$$\Delta P = -\frac{12\mu QL}{h^3}, \tag{3}$$

which is used to estimate the pressure drop, ΔP, (Pa) due to a fluid with dynamic viscosity μ (kg/m.s) passing with flow rate Q (m^3/s) through a smooth channel with length L (m) and opening h (m).

Two immediate difficulties associated with the above and similar approaches can be pointed out. The first issue is related to the subjective nature of JRC assessment as discussed earlier: different JRC values may be assigned to a rock profile by different people, which leads to different results for fluid response of a fracture. To partly overcome this problem, statistical parameters of rock profiles have been correlated to JRCs which allows a more objective assessment of roughness of rock surfaces to be made. This is discussed in detail in the next Section where a new correlation developed between the JRC and a newly proposed roughness parameter (D_{R1}) will be presented.

The second difficulty in using the above approach is related to averaging JRC values of the top and bottom walls of the fracture. To explain this issue, four synthetically generated fractures are shown in Figure 5. The top and bottom walls of these fractures are profiles taken from JRC exemplars. Each fracture is referred to as JRC_{ij} where i and j are indices indicating the top and bottom wall JRC profile number. As is seen from Figure 5, fractures shown in Figure 5(a) and 5(b) are made up from JRC profile numbers 5 and 9 but their position has been changed. This is the same for fractures in Figures 5(c) and 5(d) where JRC profiles 6 and 8 constitute the top and bottom walls of these two channels. For each fracture, the JRC value corresponding to the top and bottom wall also is given in Figure 5. The important point is that for all these fractures, the average JRC is similar and is equivalent to JRC_a=13. From Figure 5, one can immediately see a large difference between geometry of these fractures while their averaged JRC is similar.

The above simple example shows a potentially large error in estimating fracture hydraulic parameters due to averaging JRC of the top and bottom walls of a fracture without considering the geometry and position of each wall individually. The importance of this becomes clearer if it is noted that 100 fractures with combinations of JRC profiles could be generated and in some cases the average JRC of 5 fractures may be similar (for instance JRC_a=11 represents five flow channels of JRC_{210}, JRC_{39}, JRC_{48}, JRC_{57} and JRC_{66}). However, the fluid flow properties corresponding to an averaged roughness parameter may also be useful in obtaining a mean expected response of the fracture.

This work was initiated as a result of the above findings and therefore JRC flow channels were developed with a combination of pairs of JRC profiles. These generated fractures were subjected to numerical analysis of fluid flow using FLUENT software. This is discussed in the following Sections.

4 Development of JRC flow channels

In this study, bearing in mind that JRCs are meant to represent the range of real rock surface geometries, a detailed analysis of JRC profiles with respect to fluid flow was carried out. For this purpose JRC flow channels were developed where the top and bottom wall of each channel is taken to be one of the 10 JRC exemplars (see Figure 3). The digital elevation of JRC profiles extracted from the scan of printed images of the ten profiles are shown at high resolution (Rasouli, 2002).

Examples of JRC channels are shown in Figure 5, where channel JRC_{ij} represents a fracture whose top and bottom walls are JRC profiles i and j, respectively. Considering 10 JRC profiles a total of 100 JRC flow channels can be generated. It is important to note that, as per the discussion of the previous Section and from Figure 5, fluid flow response of flow channel JRC_{ij} is not necessarily similar to that of JRC_{ji}.

The 2D analysis of fluid flow requires no contact between the top and bottom wall at any point along the fracture length. In this study, in order to retain the consistency throughout the fluid analysis of different JRC flow channels a constant minimum closure distance (d_{mc}) was assumed for all 100 flow channels. This allows disregarding the influence of the minimum throat size on fluid flow behaviour and investigating the effect of channel geometry only. In Figure 6, d_{mc} is shown for a typical JRC flow channel. However, to investigate the effect of the minimum closure on flow response, the analyses were performed for three different d_{mc} of 0.01, 0.05 and 0.1cm, respectively: this is thought to be comparable with real rock fractures and the results corresponding to lesser d_{mc} indicated to be highly affected by reduced opening size. Therefore, 300 flow channels were analysed in total. It is important to note that for flow channels of JRC_{ii} where the top and bottom walls are identical in most cases, a large departure from one wall is required to satisfy the condition of $d_{mc} > 0$ (Hosseinian et al., 2010a). This is more intense in the case of JRC profiles which contain steep lag intervals and therefore it was found that within the d_{mc} range of 0.01 to 0.1cm, inclusion of the results of these profiles are inappropriate. This will not have an impact on the correlations developed here, as statistically reduction of 100 cases to 90 will not result in a loss of a general data trend.

The average JRC value corresponding to a JRC flow channel (JRC_a) is the average JRC value corresponding to the top and bottom walls. However, as also noted in the previous Section, several channels may have similar JRC_a depending on the JRC values of the top and bottom wall (for example flow channels JRC_{59} and JRC_{68} shown in Figure 5).

The aim of this paper is to analyse a large range of flow channels based on a combination of JRC profiles corresponding to real fractures and thus obtain correlations between fracture mechanical and hydraulic parameters. Analysis of these simulated fractures will be conducted numerically using FLUENT software.

5 Correlation between JRC and D_{R1}

The subjective nature of the JRC approach in characterising surface roughness was mentioned in Section 1. This was considered to be important when JRC is used to estimate fracture hydro-mechanical properties. To partly overcome this difficulty several attempts have been made to correlate JRC with some statistical parameters. For example, Tse and Cruden (1979) investigated the relationship between different statistical parameters and the JRC values given by Barton and Choubey (1977). They found that the values of root mean square (RMS) slope (Δq) are correlated with JRC and therefore presented the following correlation for estimation of JRC of real rocks:

$$\mathrm{JRC} = 32.2 + 32.47 \log \Delta q \,. \tag{4}$$

In the above equations Δ_q is defined as

$$\Delta q = \left[\frac{1}{L} \int_0^L \left(\frac{dz}{dx} \right)^2 dx \right]^{0.5}, \tag{5}$$

where L is the sampling length.

In very recent work, Rasouli and Harrison (2010) developed a new parameter for the roughness characterisation of a linear profile based on Riemannian statistics. This parameter, which is known as 1D dispersion parameter (D_{R1}) is a measure of dispersion of unit normal vectors to a profile extracted at a given sampling lag. As these unit normal vectors belong to circular data, they argued that the statistical analysis of this data is to be performed in Riemannian rather than Euclidean space. The larger the D_{R1} the rougher the rock profile will be.

Considering the potential advantages of D_{R1} as a quantitative measure of roughness, in this work we attempted to correlate this parameter with JRC: this will allow indirect estimation of JRC of a rock profile from its D_{R1} value. Accordingly, D_{R1} corresponding to 10 exemplar JRC profiles were estimated at a very small sampling size and the results are shown in Figure 7.

This figure shows that, in general, D_{R1} increases as JRC becomes larger, although this trend is not consistently followed from one JRC profile to the next larger profile: for example D_{R1} reduces from JRC=15 to JRC=17. From Figure 7 it is also seen that JRC=19 shows a larger D_{R1} compared to other profiles. Discarding the point corresponding to JRC=19, the following linear correlation fits the data best:

$$D_{R1} = 0.0069\text{JRC} + 0.1172, \tag{6}$$

or

$$\text{JRC} = \frac{\left(D_{R1} - 0.1172\right)}{0.0069}. \tag{7}$$

The results of Δq and D_{R1} estimated for some rock fractures will be compared in Section 7. However, it is important to mention that depending on the range of roughness of real rocks D_{R1} can be up-scaled to be representative of larger Mahalanobis distances (Rasouli and Harrison, 2010) but this requires further research which is not the subject of this work.

Based on the detailed discussions given in the two previous Sections, similar JRC average values for a fracture could be obtained as a result of different combinations of JRC profiles forming the top and bottom walls of the fracture. Therefore, to obtain a more representative correlation for estimating JRC with its particular applications in fluid flow analysis, here we calculated D_{R1} for different profiles with a 20cm length as being the combined length of the top and bottom walls corresponding to each JRC flow channel. As for each channel changing the position of the top and bottom walls do not change the roughness of the combined profile and a total of 55 profiles with length of 20cm were generated. Each combined profile represents an average JRC value. These profiles represent a range of geometry of rock fractures and therefore their average is expected to be a more appropriate value to be used in fluid flow analysis of rock fractures. As an example, Figure 8 shows a combined JRC profile produced from JRC_{96} flow channel. The average JRC for this profile is JRC_a=14.

All 55 combined JRC profiles were subjected to D_{R1} analysis. The plot of D_{R1} versus average JRC value corresponding to each profile is shown in Figure 9. This figure shows an increasing trend for D_{R1} as JRC increases. Also, Figure 9 demonstrates how fractures with similar averaged JRC values may differ in their roughness and therefore a range of roughness is expected for an averaged JRC value. For example, as can be found in Figure 9, D_{R1} changes between 0.1806 and 0.2238 for JRC=10 depending on which combination of JRC profiles form the top and bottom walls of the fracture. In this example, the minimum JRC_a belongs to combined profile JRC_{38} with JRC_{110} being the roughest channel. A linear correlation between D_{R1} and JRC_a is obtained in the form of

$$D_{R1} = 0.0071\text{JRC}_a + 0.1185, \tag{8}$$

or

$$\mathrm{JRC}_a = \frac{\left(D_{\mathrm{R1}} - 0.1185\right)}{0.0071}. \tag{9}$$

From Figure 9 the upper and lower bounds for JRC_a variation could be defined as:

$$\mathrm{JRC}_a(\mathrm{UL}) = \frac{\left(D_{\mathrm{R1}} - 0.1072\right)}{0.0064} \tag{10}$$

and

$$\mathrm{JRC}_a(\mathrm{LL}) = \frac{\left(D_{\mathrm{R1}} - 0.1230\right)}{0.0101}. \tag{11}$$

The mean JRC estimated from Equation 9 provides similar results to that of Equation 7 but gives a window within which the JRC may change. The above analysis shows a wide range for JRC_a depending on roughness of the two walls of the fractures and therefore it is more appropriate to assign a range, instead of a unique number, within which the JRC_a varies. This range of JRC_a can be used for fluid flow analysis which in turn determines a possible range for flow parameters, for example mean hydraulic aperture or fracture pressure drops. This will be discussed in Section 7 where applications for some real rock profiles are given.

It is to be noted that, as explained above, we propose to estimate JRC_a for a fracture from D_{R1} corresponding to the combined length of the two walls but not as an average of JRC corresponding to each wall, which is common practice. The results of our analysis indicate that JRC_a estimated from the proposed approach here provides slightly larger values for JRC of the fracture and that is a better parameter when it is linked with hydraulic parameters of the fractures.

6 Fluid flow simulation using FLUENT

All JRC flow channels were subjected to fluid flow analysis to obtain a representative range for flow response of real rock fractures. The analysis carried out for three minimum closure distances (d_{mc}) of 0.01, 0.05 and 0.10 cm. The simulations were performed numerically using FLUENT software. FLUENT has been used for fluid flow simulations of rock fractures (Nazirdoust et al., 2006; Petchsingto, 2009).

For the purpose of this study the flow in a fracture is assumed to be laminar, incompressible, isothermal, in a steady-state regime and for a viscous Newtonian fluid (Zimmerman and Bodvarsson, 1996). The continuity and momentum equations are solved In FLUENT to determine the fluid flow properties such as pressure drop or velocity magnitude. In this study, a double precision solver was used to handle the large computational effort required by fine mesh grids. Also, the SIMPLE (Semi-Implicit Method for Pressure-Linked

Equations) algorithm was utilized to estimate the pressure. The pressure-based solution available in FLUENT was utilised in this study to solve the Navier-Stokes Equations. High density grids for flow channels were generated to ensure adequate accuracy of the results using Gambit prior to simulation in FLUENT. The single phase flow of water with density of 998.2 kg/m^3 and viscosity of 0.001 kg/ms, were considered for all simulations. Considering that the fluid is incompressible (i.e. constant density) the mass flow inlet was used as the left boundary condition. Also, the pressure outlet, with zero gauge pressure at the outlet, was chosen as the right boundary condition in all models. The upper and lower solid surfaces were defined as a wall with no slip velocity boundary condition. Also, a constant flow rate of 1×10^{-7} m^3/s was used in all models. Table 1 summarises the model detail and input data used for simulations in FLUENT.

In order to perform all simulations consistently and efficiently in terms of running time, journal files were written in a text user interface (TUI) format for both Gambit and FLUENT. A journal file contains a series of TUI commands written in a text file using a text editor or generated by FLUENT as a transcript of the commands given to FLUENT. Using journal files is very useful when a series of similar simulations need to be executed, as it provides a shortcut (FLUENT Inc., 2005).

Figure 10 shows an example of a generated mesh using Gambit for one JRC flow channel. The use of high density quad meshes (total of 5000 nodes along the profile length and 25 nodes across the profile) ensures a high accuracy for the results obtained from FLUENT.

All meshes were imported to FLUENT and subjected to fluid flow analysis. Various hydraulic properties can be presented graphically in FLUENT including pressure and velocity contours. As an example, the contours of total pressure and average velocity magnitude corresponding to JRC_{37} are shown in Figure 11. Figure 11(a) shows how total pressure reduces as the fluid moves to the right, i.e. from channel inlet towards the outlet. The total pressure changes from a maximum of 1.43 pa at the inlet to a minimum of 0 Pa when it arrives at the channel outlet: i.e. a total pressure drop of 1.43 Pa. The small range of pressure values are due to a small value of flow rate assumed for the simulations. This is unimportant in this study as the main objective of this work is to compare the response of different JRC flow channels. However, one may normalise the pressure values by dividing them by pressure drop of a smooth channel with its opening being equivalent to the minimum closure distance (d_{mc}) of a given JRC flow channel. Considering that the length of all JRC flow channels are identical (i.e. 10cm) and for a unit width, the pressure drop corresponding to three d_{mc} of 0.01, 0.05 and 0.1 cm would be obtained from equation 3 as 120, 0.96 and 0.12 Pa, respectively.

In Figure 11(b) the contours of velocity magnitude shown for a small interval of this fracture, where the maximum velocity occurs, indicates a variation range between 0 and 0.001467 m/s. It is seen from this figure, as expected, that larger velocities occur at lower openings along the channel with its maximum being at the point where the opening is equal to d_{mc}, i.e. the lowest opening along the fracture. Also, considering the flow is laminar with a hyperbolic velocity profile it is clear that getting closer to the channel walls, the velocity reduces and finally becomes zero.

7 Data analysis of JRC flow channels

In this Section, the results of fluid flow analysis of JRC flow channels performed using FLUENT are presented. However, in order to interpret the results given here, it is important to note that in this study we have considered a constant minimum closure distance (d_{mc}) for all JRC flow channels. This was to discard the significant impact of the maximum reduction in channel size on flow response and to allow an investigation of the effect of channel roughness on flow response to be made. Therefore, it is expected that as the JRC flow channel walls become rougher, i.e. larger JRC_a, the mechanical aperture of the channel increases, which in general results in a lesser pressure drop or average fluid velocity, assuming that flow rate is constant. In other words, in these presented JRC flow channels the maximum distance between the two walls is not constant but changes based on the assumed d_{mc}.

The pressure drop for JRC flow channels was extracted directly from FLUENT simulations. This data was used to estimate the hydraulic aperture (h_H) from back analysis of the Cubic law given in Equation 3.

Figure 12 shows, as an example, the results of mechanical aperture calculated for JRC flow channels. In this example the minimum closure distance is d_{mc}= 0.01cm. As is seen from this figure, h_m increases as JRC_a becomes larger. The power correlation fit to the data in Figure 12 allows estimating h_m from JRC_a. A window shown in Figure 12 determines the range of data variation for a mechanical aperture. The mechanical aperture can also be estimated from the ratio A/L, where A is the area between the two walls of the fracture and L is fracture length (Hosseinian et al., 2010b).

Similar trends were observed for the other two cases with d_{mc}= 0.05cm and d_{mc}= 0.1cm, where mechanical aperture increases with d_{mc}. Therefore the following correlations were based on the normalised aperture h_m^n (i.e. the aperture divided by the d_{mc}):

$$h_m^n = 1 + \frac{0.05}{d_{mc}} JRC_a^{0.52}, \tag{12}$$

$$h_{\mathrm{m}}^{n}\left(\begin{matrix}\mathrm{UL}\\ \mathrm{LL}\end{matrix}\right)=h_{\mathrm{m}}^{n}\pm\frac{0.10}{d_{\mathrm{mc}}}, \tag{13}$$

where $h_{m}^{n}\left(\begin{matrix}\mathrm{UL}\\ \mathrm{LL}\end{matrix}\right)$ gives the upper and lower limits for changes in mechanical aperture.

An increase in d_{mc} is expected to increase the hydraulic aperture but with a different trend to that of the mechanical aperture. Figure 13 shows the plots of hydraulic aperture versus JRC_a corresponding to three d_{mc} of 0.01, 0.05, and 0.1cm, respectively. The power correlations fit to the data are shown in Figure 13. Also, from this figure it is seen that the data vary within a window of ± 0.012 to ± 0.03 and to ± 0.04 from Figure 13(a) to 13(c). From correlations obtained in Figure 13, the following correlation was developed for h_{H}^{n} as a function of JRC_a and d_{mc}:

$$h_{\mathrm{H}}^{n}=1+\frac{0.06}{d_{\mathrm{mc}}^{0.58}}\mathrm{JRC}_{a}^{0.60}, \tag{14}$$

with data being distributed in a window of

$$h_{\mathrm{H}}^{n}\left(\begin{matrix}\mathrm{UL}\\ \mathrm{LL}\end{matrix}\right)=h_{\mathrm{H}}^{n}\pm\left(\frac{0.13}{d_{\mathrm{mc}}^{0.50}}\right). \tag{15}$$

In these equations d_{mc} is in cm. Equation 14 shows that regardless of roughness of the JRC flow channel, if d_{mc} becomes very large the normalised hydraulic aperture approaches unity, i.e. hydraulic aperture will be equivalent to d_{mc}.

The plot of h_{m} versus h_{H} shown in Figure 14 shows a gradual increase in h_{H} as h_{m} increases. This figure shows the results corresponding to d_{mc} = 0.01cm, however, similar trends were observed for another two cases where d_{mc} is equal to 0.05 cm and 0.10 cm. Accordingly, power correlation was derived between the normalised mechanical and hydraulic aperture:

$$h_{\mathrm{H}}^{n}=\frac{1.77}{d_{\mathrm{mc}}^{0.35}}h_{\mathrm{m}}^{0.87}d_{\mathrm{mc}}^{0.2}. \tag{16}$$

A variation window similar to equation 15 was found to be appropriate for Figure 14, which shows the range of changes of h_{H} as a function of h_{m}.

Figure 15 presents the plots of $(h_{\mathrm{H}}/h_{\mathrm{m}})^3$ versus JRC_a for different flow channles. The results indicate that larger channel roughness leads to a lesser hydraulic conductivity. Also, comparing Figures 15(a) to 15(c) the larger the d_{mc} the larger the channel permeability. The best fit to the data is shown in Figure 15. Generalising the results obtained from this figure, a correlation between JRC flow channels permeability as a function of JRC_a and d_{mc} is obtained in the form of

$$\left(\frac{h_H}{h_m}\right)^3=\left(1-0.03d_{\mathrm{mc}}^{-0.565}\right)^{\mathrm{JRC}_a}. \tag{17}$$

As this equation shows, and is seen from Figure 15, permeability reduces significantly when d_{mc} get closer to zero and approaches unity for very large values of d_{mc} regardless of the channel roughness.

For real rocks JRC_a can be estimated in relation to D_{R1} from equation 9, in order to obtain permeability through Equation 17.

A Plot of permeability as a function of h_m/σ, where σ is the standard deviation corresponding to JRC_a can also be produced (Yeo, 2005). Figure 16 shows such a plot for three different d_{mc}. This plot shows how the range of data distribution increases as d_{mc} or h_m increases. In general, permeability increases as the ratio of h_m/σ becomes larger but this is more consistent for d_{mc} = 0.10 cm compared to the other two smaller openings and for ratios of h_m/σ greater than approximately 3. The results presented here are similar to those reported by other researchers (e.g. Liu, 2005; Yeo, 2005; Ge, 1997; Renshaw, 1995 and Patir and Cheng, 1978).

From Figure 16, a correlation between permeability of JRC flow channels and h_m/σ is obtained as

$$\left(\frac{h_H}{h_m}\right)^3 = 1 - 2.25\left(\frac{\sigma}{h_m}\right), \tag{18}$$

where the data changes within a window with a lower limit of

$$\left(\frac{h_H}{h_m}\right)^3_{LL} = 1 - \left(\frac{\sigma}{h_m}\right), \tag{19}$$

and an upper limit of

$$\left(\frac{h_H}{h_m}\right)^3_{UL} = 1 - 3.70\left(\frac{\sigma}{h_m}\right). \tag{20}$$

From equation 18 to 20 it is seen that as h_m/σ becomes larger the channel roughness reduces and therefore permeability increases. For very large values of h_m/σ the permeability approaches unity (i.e. $h_H = h_m$), which corresponds to a smooth channel. On the other hand, as roughness increases the deviation between hydraulic and mechanical aperture increases.

The results of a normalised pressure drop (ΔP_n) for JRC flow channels are plotted in Figure 17 for data corresponding to channels having d_{mc} = 0.10 cm, with a larger range of values compared to the other two channel openings. This figure shows a reduction in pressure drop as the average JRC of the channel increases: this is due to the fact that the d_{mc} is constant in all cases but the two walls depart further away from each other. Also, a variation range between approximately +0.10 and -0.05 is observed for pressure drop changes.

A similar trend was observed for JRC flow channels with d_{mc}= 0.01cm and 0.05 cm and accordingly the following correlation was developed between pressure drop and JRC_a as a function of d_{mc}:

$$\Delta P_n = d_{mc} + (1 - d_{mc})\left(1 - 0.15 d_{mc}^{-0.32}\right)^{JRC_a} . \quad (21)$$

where pressure drop changes within a window of

$$\Delta P_{n,UL} = \Delta P_n + d_{mc}$$
$$\Delta P_{n,LL} = \Delta P_n - \frac{d_{mc}}{2} . \quad (22)$$

In this equation d_{mc} is in cm. Equation 21 indicates that, regardless of the roughness of the flow channel, pressure drop increases significantly when d_{mc} becomes very small, but approaches unity if d_{mc} increases to a large volume: the latter corresponds to the pressure drop of a smooth channel with opening d_{mc}. As can be seen Equation 21 satisfies all boundary conditions and appears to give a good estimation of pressure drop within rock fractures. This will be assessed in Section 7, where applications of this correlation in some rock fractures are presented.

Several similar correlations could be developed between various geometrical and hydraulic parameters of JRC flow channels depending on the particular application required. However, the results of JRC flow channels show how it may be possible to obtain a more generalised flow response of real rock surfaces by analysing a large range of simulated fractures.

Using the correlations above developed, one may estimate the average JRC_a values of the fracture walls using correlations 4 or 9 from corresponding Δq or D_{R1} values. Then, the hydraulic aperture can be calculated from equation 14 and the pressure drop can be estimated through equation 21.

It is important to note the input parameters used (see Table 1) to derive these correlations. Therefore, if a fracture is analysed with properties different from those used here, the flow parameters should be modified accordingly.

These correlations will be applied to the analysis of several real rock fractures in the next Section.

8 Analysis of rock fractures

In order to examine the range of applications of the correlations developed in the previous Section, several real rock fractures with a wide range of average roughness were studied using these correlations. Here the results corresponding to 9 fractures taken from a granite block are presented and compared with those obtained from direct simulation of these fractures using FLUENT.

In order to demonstrate the applicability of the correlations developed here, we tried to extract 2D profiles with wide a range of roughness along different directions across the Granite block. The geometry of 9 fractures F1 to F9 used for this study is shown in Figure 18. The length of all fractures was taken to be 10 cm, similar to the JRC flow channels. The minimum closure distance (d_{mc}) was different for these fractures (ranging from 0.03 to 0.10 cm). Selection of smaller d_{mc} was found to be inappropriate for illustration purposes as in this situation the fracture response will be significantly affected by sudden reduction of the fracture opening. In Table 2, d_{mc}, together with statistical parameters Δq and D_{R1} introduced in Section 4 estimates for these fractures are shown. It is interesting to note that fracture F5 and F6 has a similar roughness (i.e. D_{R1}) but their d_{mc} is different: it is 0.10 and 0.07 for fracture F5 and F6, respectively. Data in Table 2 was used to estimate JRC_a for these fractures from Equations 4 and 9, respectively, and these values are also shown in Table 2 and plotted in Figure 19. From this figure it appears that for these fractures D_{R1} generally overestimates JRC_a compared to those obtained from Δq.

Fractures F1 to F9 were subjected to FLUENT analysis and also correlations developed in the previous Section were applied to estimate their flow parameters. In Figure 20(a) the normalised mechanical apertures (h_m^n) for these fractures estimated through correlations 12 is compared against those obtained from FLUENT simulations. Similarly, Figure 20(b) shows hydraulic apertures (h_H^n) corresponding to fractures estimated from correlation 14 and simulations. In Figure 20, the upper and lower limits for apertures obtained from correlations 13 and 15, respectively, are marked. This figure indicates very good agreement between the results obtained through the developed correlations and simulation as most of the data distributed alongside the line with a 45° slope and is within the expected limits.

Figure 21 presents the results of normalised pressure drop for fractures F1 to F9 obtained from simulation and correlation 21. The expected limits for data variation estimated from correlation 22 are marked in Figure 21. This Figure shows a good prediction made by the correlation developed for fracture pressure drop based on JRC flow channels.

The results of Figures 20 and 21 demonstrate the applications of correlations developed based on JRC flow channels to estimate hydraulic parameters of rough rock fractures. In Figure 22 the normalised mechanical and hydraulic apertures estimated for given fractures are plotted versus their roughness parameter D_{R1}. From this figure, it is seen that generally both mechanical and hydraulic apertures increase from fracture F1 to F9, i.e. as fractures become rougher. Corresponding to this, the pressure drop reduces as we move from fracture F1 to F9, as depicted in Figure 23. In Figure 23 it is interesting to note that fracture F5 indicates to a larger pressure drop than F6 while their roughness is identical. Looking at the geometry of

these two fractures in Figure 18 it is seen that fracture F5 experiences a large reduction in its opening which results in a larger aperture and hence pressure drop.

In Figure 24, the plot of fracture permeability is shown with respect to D_{R1}. From this figure it is expected that in general fracture permeability reduces from F1 to F9 due to a lesser area being exposed to fluid flow when the fracture becomes rougher. This figure indicates a larger permeability for fracture F5 than F6. This is due to the fact that fracture F5 has larger d_{mc} compared to F6 (see Table 2) which results in a larger transmissivity.

The above discussions and conclusions demonstrate the capability of correlations in considering different factors (e.g. minimum closure distance, roughness, etc) in order to estimate hydraulic parameters of fractures. Further investigations are currently being carried out to expand such applications.

Conclusions

This paper presented the difficulties associated with using currently available formulae for fluid flow analysis of rock fractures which are correlated with JRC. Through simple examples it has been shown how different flow channels with different geometries could have a similar averaged roughness value (or JRC). Also, it was illustrated how changing the position of the top and bottom walls of a fracture may lead to a different fracture geometry and thus different flow responses while averaged roughness is identical in both cases.

The analysis of combined JRC profiles resulted in a more generalised correlation between averaged JRC_a and roughness parameter D_{R1}. D_{R1} for a real rock fracture could be used to estimate average JRC_a. The results indicated how wide the range of JRC_a could be, depending on which combination of JRC profiles were presented as the top and bottom wall of the fracture.

From analysis of JRC flow channels various correlations between channel geometrical and hydraulic properties were developed. In order to only investigate the roughness effect, the minimum closure distance for the channels was kept constant. The results showed how pressure drop reduces as average JRC_a increases and this corresponds to an increase in fracture mechanical and hydraulic apertures.

Comparing the results obtained for 9 real fractures from correlations and direct simulation using FLUENT software, we have demonstrated the applicability of a proposed formulae. Further work is ongoing to study additional real fractures.

References

Barton , N., 2007, Rock quality, seismic velocity, attenuation and anisotropy: London: Taylor & Francis Group

Barton, N., and Choubey, V., 1977, The shear strength of rock joints in theory and practice: Rock Mechanics and Rock Engineering, v. 10, p. 1-54.

Barton, N., and de Quadros, E.F., 1997, Joint aperture and roughness in the prediction of flow and groutability of rock masses: International Journal of Rock Mechanics and Mining Sciences, v. 34, p. 252.e1-252.e14.

Barton, N., Bandis, S., and Bakhtar, K., 1985, Strength, deformation and conductivity coupling of rock joints: International Journal of Rock Mechanics and Mining Sciences & Geomechanics Abstracts, v. 22, p. 121-140.

Crandall, D., Ahmadi, G., and Smith, D., 2010a, Computational Modeling of Fluid Flow through a Fracture in Permeable Rock: Transport in Porous Media, v. 84, p. 493-510.

Crandall, D., Bromhal, G., and Karpyn, Z.T., 2010b, Numerical simulations examining the relationship between wall-roughness and fluid flow in rock fractures: International Journal of Rock Mechanics and Mining Sciences, v. 47, p. 784-796.

Fluent Inc., 2005, FLUENT 6.3 User's Guide. Chapter 3: Text User Interface (TUI). P.1-2

Ge, S., 1997, A governing equation for fluid flow in rough fractures: Water Resources. Res., v. 33, p. 53-61.

Giacomini, A., Buzzi, O., Ferrero, A.M., Migliazza, M., and Giani, G.P., 2008, Numerical study of flow anisotropy within a single natural rock joint: International Journal of Rock Mechanics and Mining Sciences, v. 45, p. 47-58.

Hosseinian, A., Rasouli, V., and Utikar, R., 2010a, Fluid flow response of JRC exemplar profiles, European Rock Symposium (EUROCK 2010): Switzerland: Lausanne, Taylor & Francis Group.

Hosseinian, A., Rasouli, V., and Bahrami, H., 2010b, Analytical and numerical analysis of fluid flow through rough natural fracture profiles, 44th US Rock Mechanics Symposium and 5th U.S.-Canada Rock Mechanics Symposium: Salt Lake City, UT.

Jaeger, J.C., and Cook, N.G.W., and Zimmerman, R.W., 2007, Fundamentals of Rock Mechanics (4th Edition), John Wiley & Sons.

Koldiz , O., 2001, Non-linear flow in fractured rock: Int. J. Num. Meth. For Heat & Fluid Flow, v. 11, P. 547-575.

Koyama, T., Li, B., Jiang, Y., and Jing, L., 2009, Numerical modelling of fluid flow tests in a rock fracture with a special algorithm for contact areas: Computers and Geotechnics, v. 36, p. 291-303.

Kulatilake, P.H.S.W., 2008, Quantification of aperture and relations between aperture, normal stress and fluid flow for natural single rock fractures: Geotechnical and geological engineering, v. 26, p. 269.

Liu, E., 2005, Effects of fracture aperture and roughness on hydraulic and mechanical properties of rocks: implication of seismic characterisation of fractured reservoir: J. Geophys & Eng, p.38-47

Liu, H., and Sterling, R., 1990, Statistical description of the surface roughness of rock joints, The 31th US Symp. Rock Mech.

Nazridoust, K., Ahmadi, G., and Smith, D.H., 2006, A new friction factor correlation for laminar, single-phase flows through rock fractures: Journal of Hydrology, v. 329, p. 315-328.

Olsson, R., and Barton, N., 2001, An improved model for hydromechanical coupling during shearing of rock joints: International Journal of Rock Mechanics and Mining Sciences, v. 38, p. 317-329.

Patir, N., and Cheng, H.S., 1978, An average flow model for determining effects of three dimensional roughness on partial hydrodynamic lubrication: J Lubr Tech, v. 100, p. 12-17.

Petchsingto, T., and KARPYN, Z.T., 2009, Deterministic Modeling of Fluid Flow through a CT-scanned Fracture Using Computational Fluid Dynamics: Energy sources. Part A, Recovery, utilization, and environmental effects, v. 31, p. 897.

Petchsingto, T., and KARPYN, Z.T., 2009, Deterministic Modeling of Fluid Flow through a CT-scanned Fracture Using Computational Fluid Dynamics: Energy sources. Part A , Recovery, utilization, and environmental effects, v. 31, p. 897.

Rasouli , V., 2002, Application of Riemannian multivariate statistics to the analysis of fracture surface roughness: PhD thesis, Imperial College, London.

Rasouli, V., and Harrison, J.P., 2001, Is the observational method of roughness determination trustworthy? , Proc. ISRM Int. Symp. Eurock 2001: Espoo, Finland. , p. 277-282.

Rasouli, V., and Harrison, J.P., 2010, Assessment of rock fracture surface roughness using Riemannian statistics of linear profiles: International Journal of Rock Mechanics and Mining Sciences, v. 47, p. 940-948.

Renshaw, C.E., 1995, On the relationship between mechanical and hydraulic apertures in rough-walled fractures: J. Geophys. Res., v. 100, p. 24629-24636.

Sarkar, S., 2002, Fluid Flow Simulation in Fractured Reservoirs, *in* Earth Resources Laboratory, M.I.o.T., ed.: Cambridge

Scesi, L., and Gattinoni, P., 2007, Roughness control on hydraulic conductivity in fractured rocks: Hydrogeology Journal, v. 15, p. 201-211.

Tse, R., and Cruden, D.M., 1979, Estimating joint roughness coefficients: International journal of rock mechanics and mining sciences & geomechanics abstracts, v. 16, p. 303-307.

Wayne, N.R., Schechter, D.S., and Thompson, L.B., 2006, Naturally Fractured Reservoir Characterization: SPE

Yeo, I., and Ge, S., 2005, Applicable range of the Reynolds equation for fluid flow in a rock fracture: Geosciences Journal, v. 9, p. 347-352.

Zimmerman, R.W., and Bodvarsson, G.S., 1996, Hydraulic conductivity of rock fractures: Transport in Porous Media, v. 23, p. 1-30.

Zimmerman, R.W., Kumar, S., and Bodvarsson, G. S., 1991, Lubrication theory analysis of the permeability of rough-walled fractures: International Journal of Rock Mechanics and Mining Sciences & Geomechanics Abstracts, v. 28, p. 325-331.

List of Tables

List of Figures

Table 1

Click here to download Table: Fluid Flow_210610_Tables_1.eps

Boundary Conditions:	
Inlet	Mass flow inlet
Outlet	Pressure outlet
Fluid:	Water
Density (kg/m^3)	998.2
Viscosity (kg/ms)	0.001
Flow rate (m^3/s)	1×10^{-7}

Table 2

Click here to download Table: Fluid Flow_210610_Tables_2.eps

Fracture	d_{mc} (cm)	D_{R1}	JRCa (from D_{R1})	JRC_a (from Δq)
F1	0.054	0.1652	6.58	5.06
F2	0.034	0.1700	7.25	5.55
F3	0.076	0.2271	15.30	9.08
F4	0.073	0.2290	15.56	10.36
F5	0.102	0.2352	16.43	10.36
F6	0.071	0.2347	16.37	11.48
F7	0.077	0.2458	17.93	11.04
F8	0.071	0.2500	18.52	11.48
F9	0.067	0.2612	20.00	13.63

Figure 1

Click here to download Figure: Fluid Flow_210610_Figs_ 1.eps

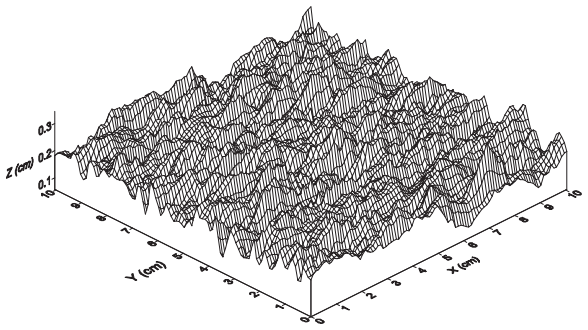

Figure 2
Click here to download Figure: Fluid Flow_210610_Figs_ 2.eps

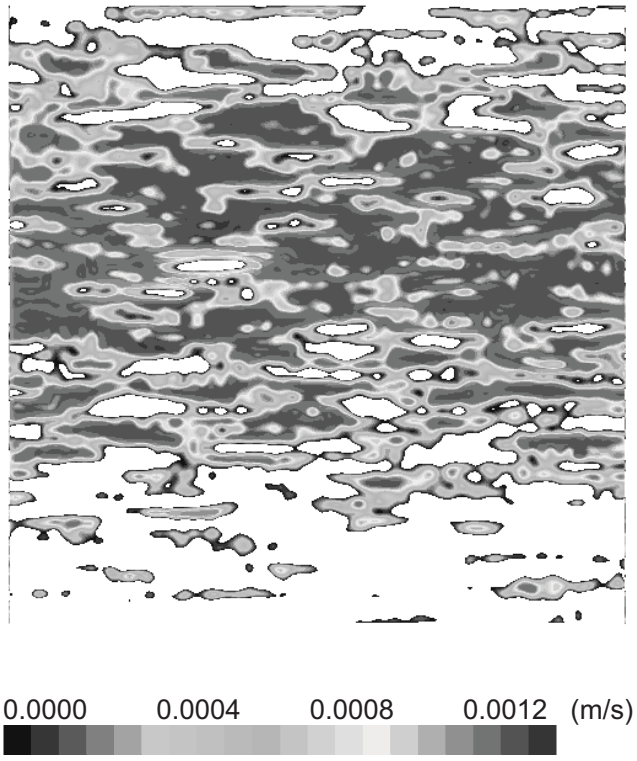

(a)

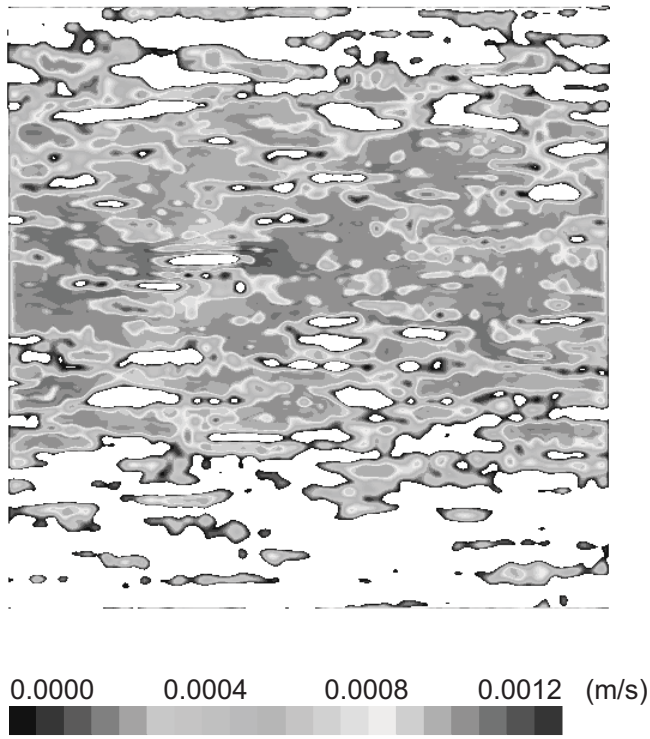

(b)

Figure 3
Click here to download Figure: Fluid Flow_210610_Figs_ 3.eps

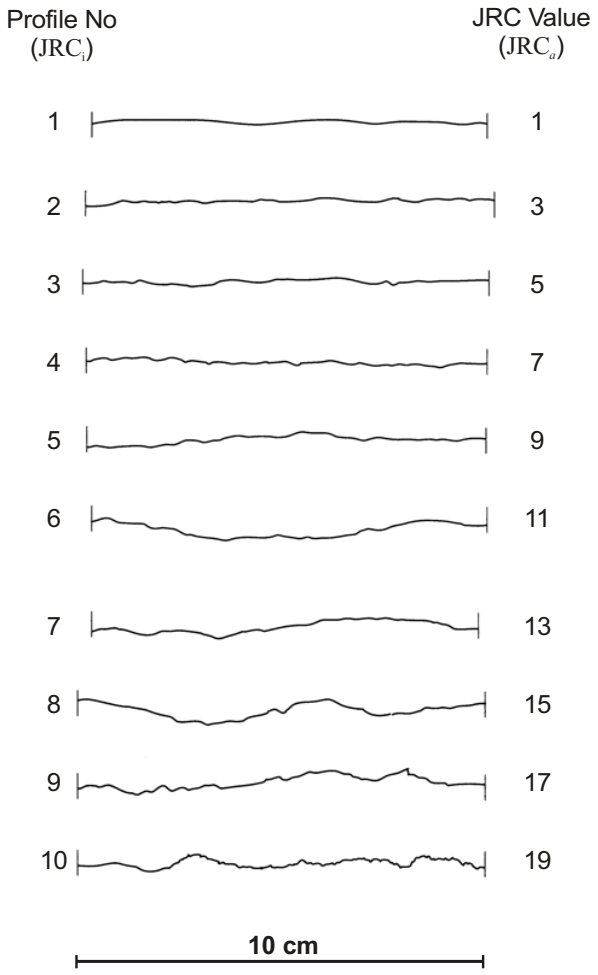

Figure 4

Click here to download Figure: Fluid Flow_210610_Figs_ 4.eps

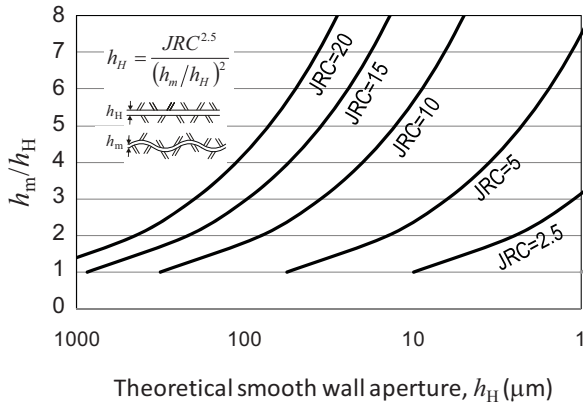

Figure 5
Click here to download Figure: Fluid Flow_210610_Figs_ 5.eps

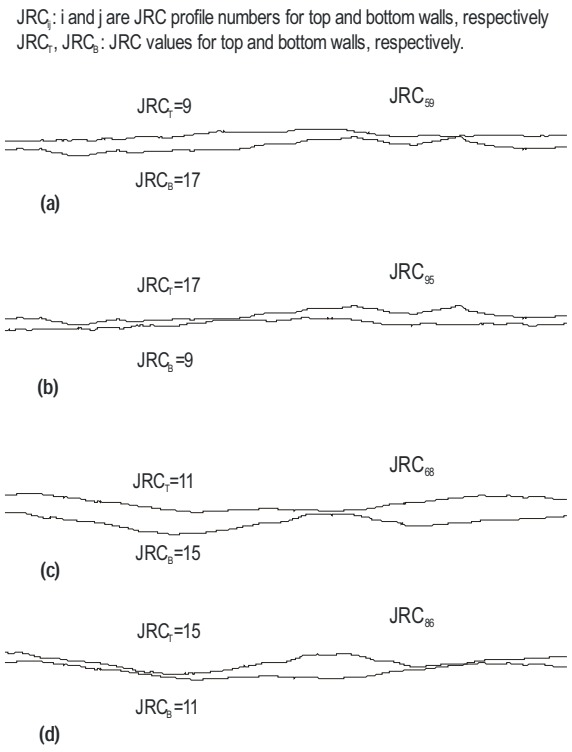

JRC average (JRC$_a$) is 13 for all four generated JRC flow channels

Figure 6

Click here to download Figure: Fluid Flow_210610_Figs_ 6.eps

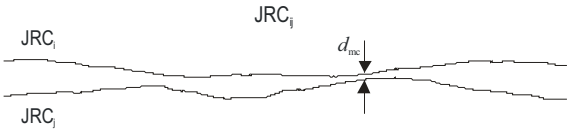

Figure 7

Click here to download Figure: Fluid Flow_210610_Figs_ 7.eps

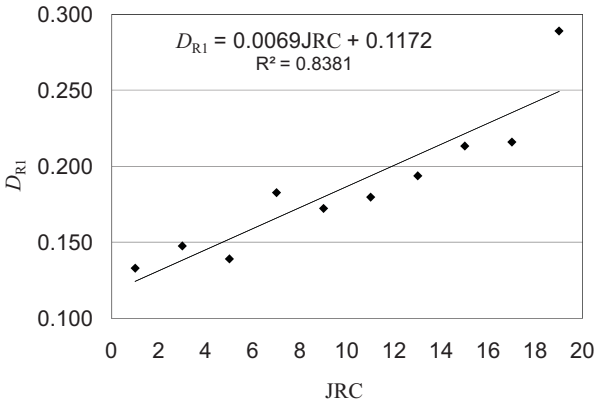

Figure 8

Click here to download Figure: Fluid Flow_210610_Figs_ 8.eps

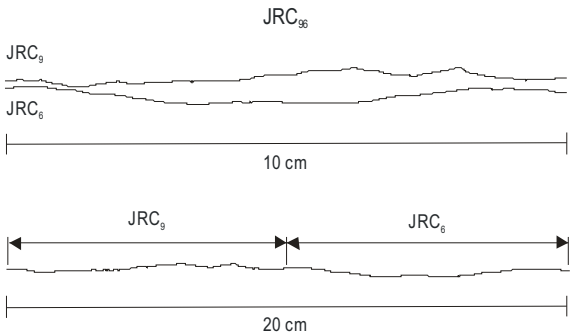

A combine JRC profile produced from top and bottom walls of a JRC flow channel

Figure 9

Click here to download Figure: Fluid Flow_210610_Figs_ 9.eps

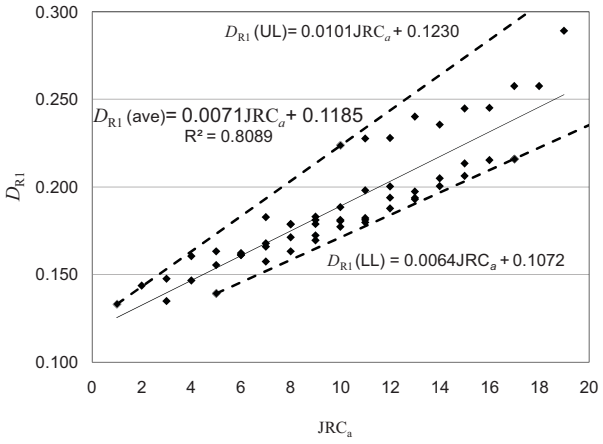

Figure 10
Click here to download Figure: Fluid Flow_210610_Figs_ 10.eps

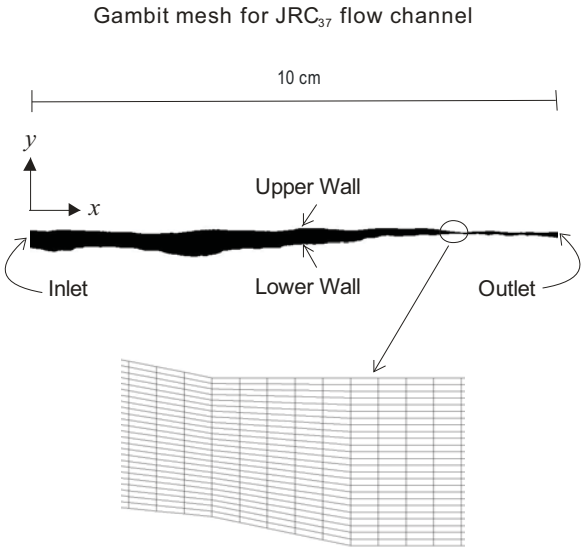

Mesh includes 5,000 nodes in x and 25 nodes in y direction

Figure 11
Click here to download Figure: Fluid Flow_210610_Figs_ 11.eps

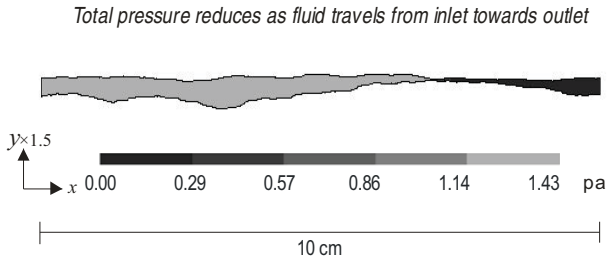

(a)

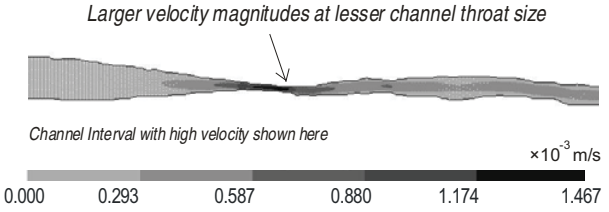

(b)

Figure 12
Click here to download Figure: Fluid Flow_210610_Figs_ 12.eps

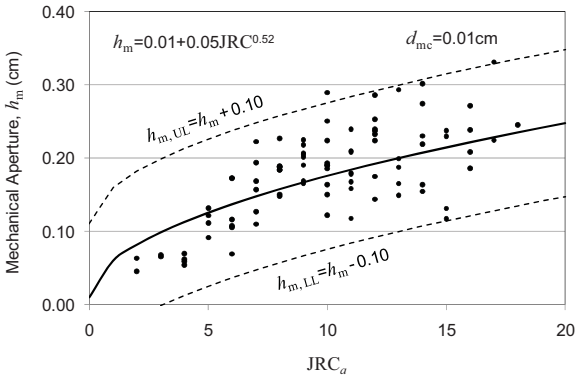

Figure 13

Click here to download Figure: Fluid Flow_210610_Figs_ 13.eps

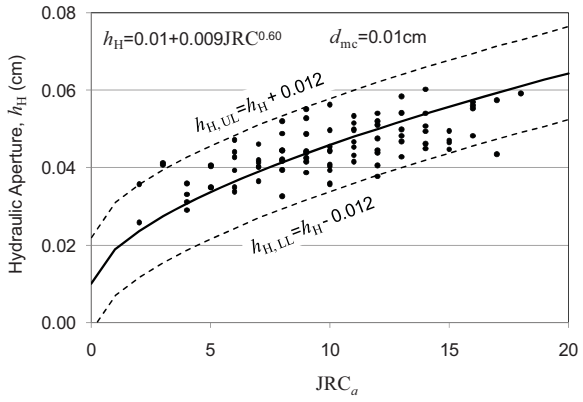

(a)

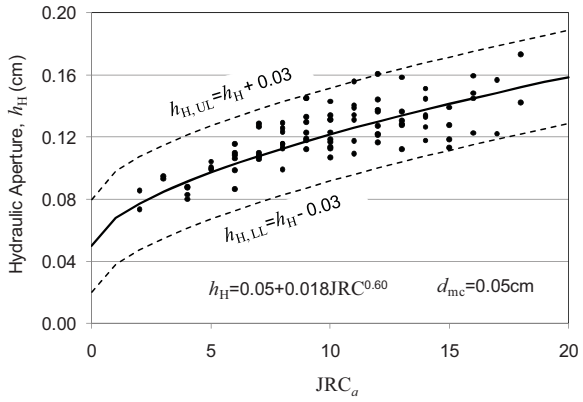

(b)

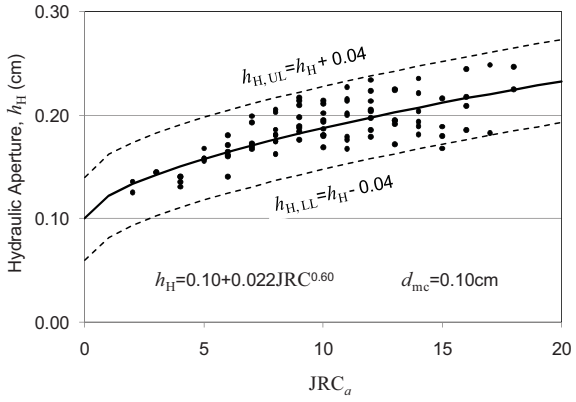

(c)

Figure 14

Click here to download Figure: Fluid Flow_210610_Figs_ 14.eps

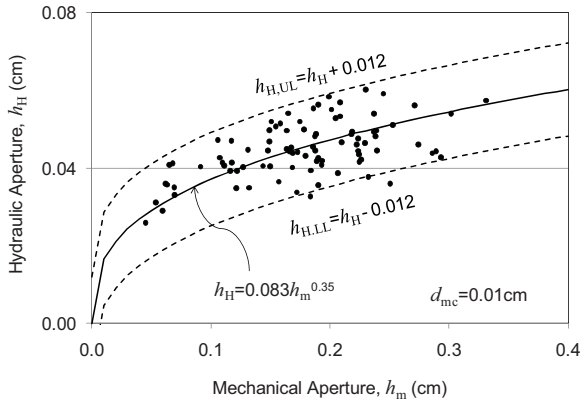

Figure 15
Click here to download Figure: Fluid Flow_210610_Figs_ 15.eps

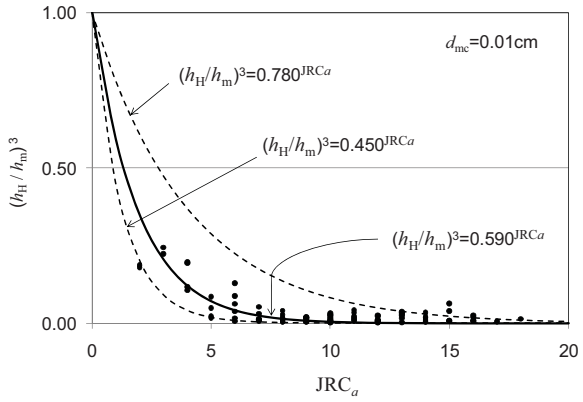

(a)

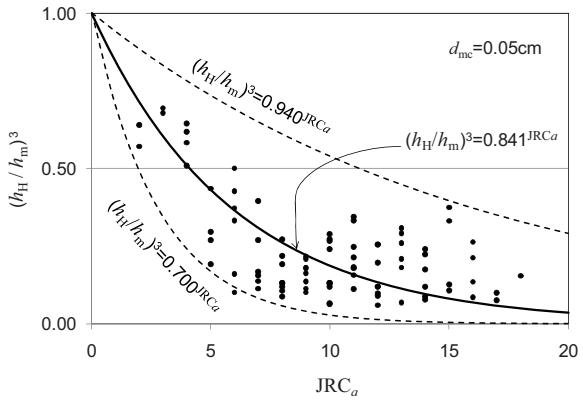

(b)

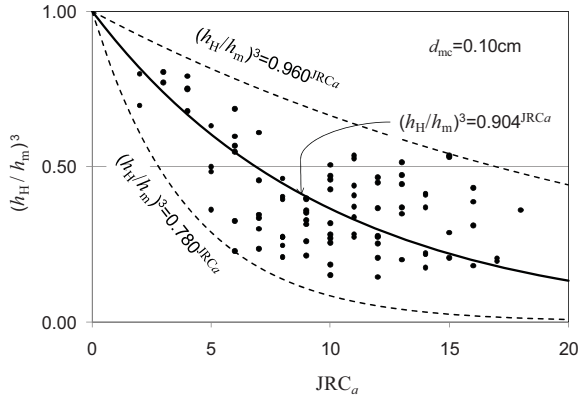

(c)

Figure 16

Click here to download Figure: Fluid Flow_210610_Figs_ 16.eps

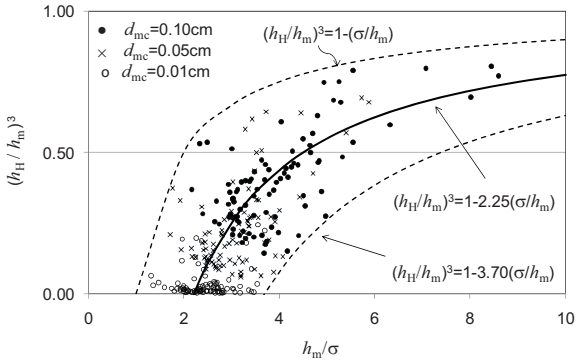

Figure 17

Click here to download Figure: Fluid Flow_210610_Figs_ 17.eps

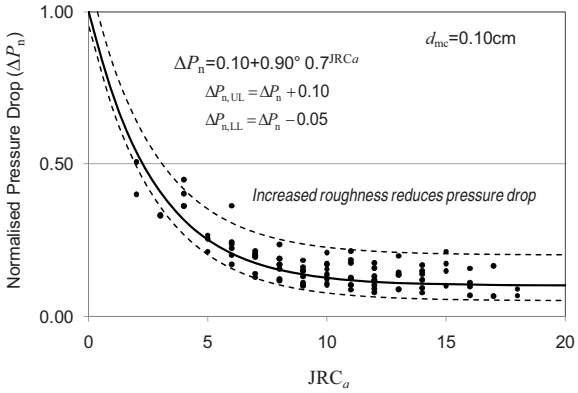

Figure 18
Click here to download Figure: Fluid Flow_210610_Figs_ 18.eps

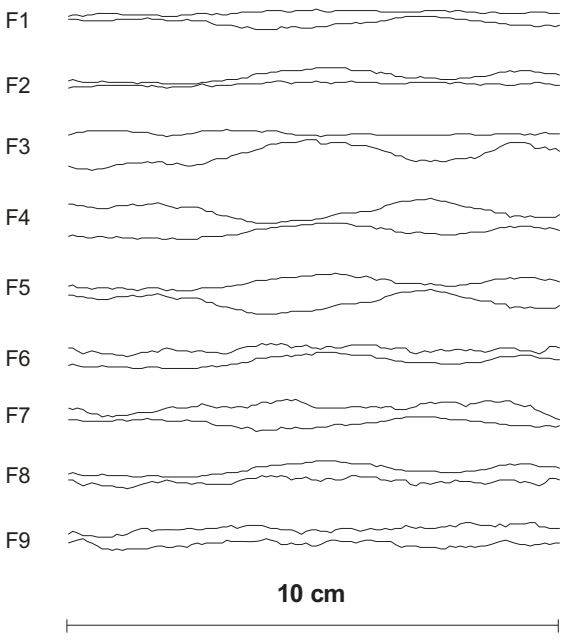

Figure 19
Click here to download Figure: Fluid Flow_210610_Figs_ 19.eps

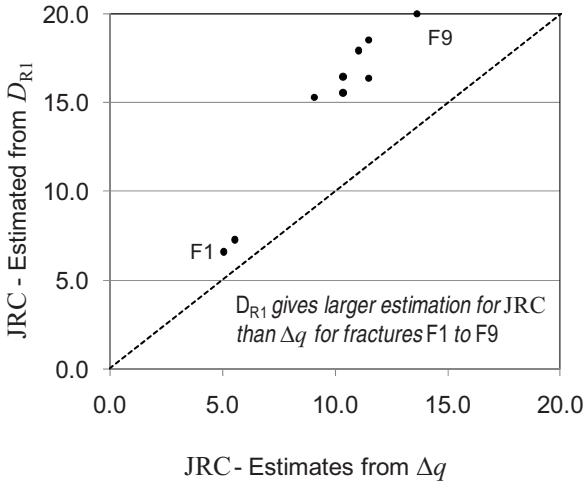

Figure 20
Click here to download Figure: Fluid Flow_210610_Figs_ 20.eps

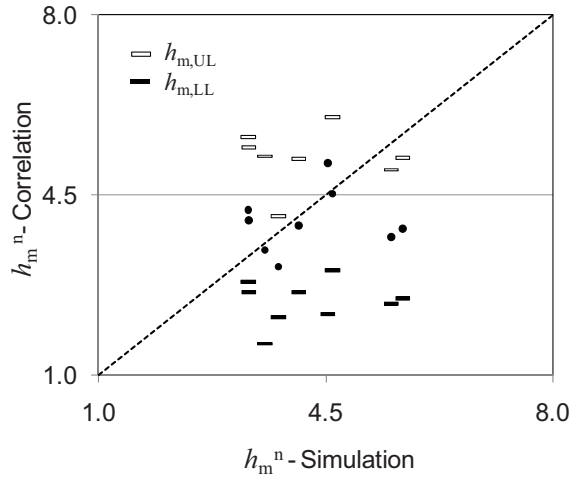

(a)

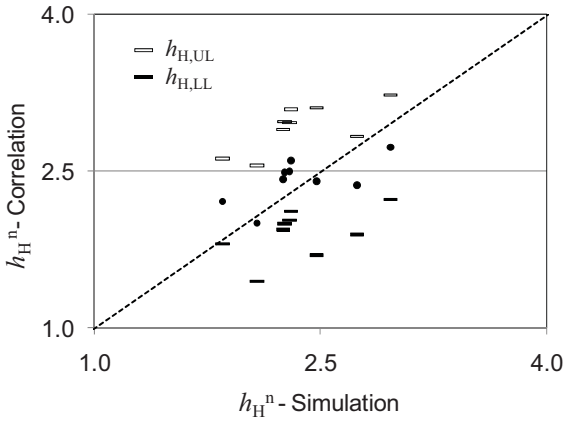

(b)

Figure 21
Click here to download Figure: Fluid Flow_210610_Figs_ 21.eps

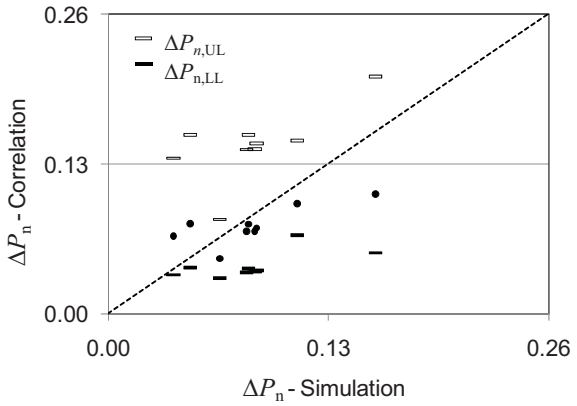

Figure 22
Click here to download Figure: Fluid Flow_210610_Figs_ 22.eps

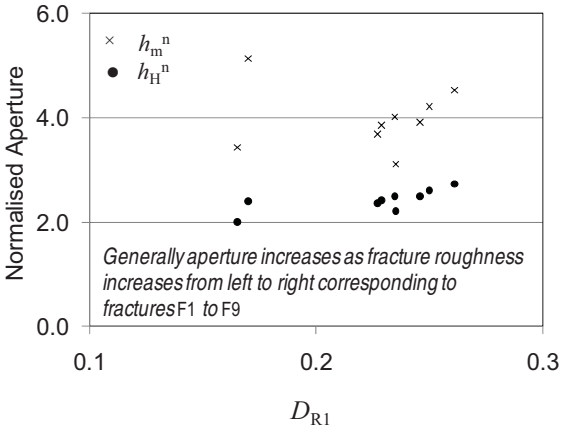

Figure 23

Click here to download Figure: Fluid Flow_210610_Figs_ 23.eps

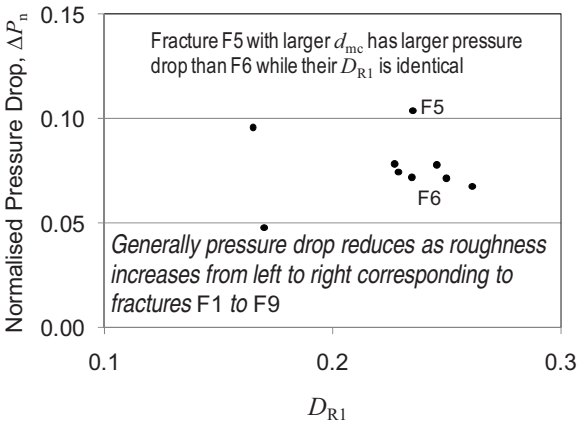

Figure 24

Click here to download Figure: Fluid Flow_210610_Figs_ 24.eps